AIMS Mathematics, 11(3): 5992–6018.
DOI:10.3934/math.2026248
Received: 23 December 2025
Revised: 12 February 2026
Accepted: 26 February 2026
Published: 10 March 2026

https://www.aimspress.com/journal/Math

Research article

Data-driven modeling and simulation of Caputo–Fabrizio fractional order shingles disease model

Aziz Khan[1], Aiman Mukheimer[1], Thabet Abdeljawad[1,2,3,*] and Rajermani Thinakaran[4]

[1] Department of Mathematics and Sciences, Prince Sultan University, P. O. Box 66833, 11586 Riyadh, Saudi Arabia

[2] Department of Fundamental Sciences, Faculty of Engineering and Architecture, Istanbul Gelisim University, Avcilar, 34310, Istanbul, Turkey

[3] Department of Medical Research, China Medical University, Taichung, 40402, Taiwan

[4] Faculty of Data Science and Information Technology, INTI International University, Negeri Sembilan, Malaysia

* **Correspondence:** Email: tabdeljawad@psu.edu.sa.

Abstract: This study deals with Caputo–Fabrizio (CF) fractional-order shingles disease model to capture the intrinsic memory and nonlocal properties that govern the progression of herpes zoster within a population. The model is organized into interacting epidemiological compartments and its mathematical soundness is confirmed by establishing both the existence and stability of results through fixed-point theory and fractional theory. To approximate the model behavior, a high accuracy numerical method based on the Lagrangian interpolation technique is constructed, allowing smooth reconstruction of fractional trajectories and robust behavior of nonlocal operators. Complementing this numerical context, an artificial neural network technique is used and trained using the Levenberg–Marquardt optimization algorithm, enabling efficient learning of disease patterns and authentication of numerical fidelity. Performance indicators, involving regression, training test, error histogram, and convergence features, confirm the reliability of the ANN-supported evaluation. The combined modeling, numerical, and computational analysis offers a comprehensive estimation of the fractional dynamics governing shingles transmission, presenting deeper insights into disease evolution and displaying the capacity of fractional operators and intelligent systems to enhance health risk predictive epidemiological modeling.

Keywords: Caputo–Fabrizio operator; neural networks; shingles diseases; numerical method; training fit; Levenberg–Marquardt
Mathematics Subject Classification: 26A33, 34A08, 34A12, 34A34

1. Introduction

Shingles, medically represented to as Herpes Zoster, is a viral reactivation condition caused by the varicella-zoster virus (VZV), the same agent dependable for primary chickenpox infection. Historical explanations of shingles-like dermatomal epidemics appear in classical Greek and Roman medical literature, showing that the disease has been familiar for centuries as a distinct clinical entity [1]. After initial infection, typically striking during childhood, VZV determines lifelong inactivity in the dorsal root or cranial nerve ganglia, and numerous immunological studies have shown that repetition can occur under conditions of weakened immunity, aged, psychological stress, or immune suppressant drug therapy [2]. Clinically, the disease develops through prodromal, eruptive, and healing stages, starting with fever, neuro pathic scratchy, and burning feelings along sensory nerves, respected by unilateral vesicular lesions that may continue for weeks [3]. A major clinical impediment is post-herpetic neuralgia (PHN), a chronic pain condition that may restart long after visible lesions have resolved, severely impacting patient quality of life [4]. Although active vaccines exist, population-wide epidemiological data reveal that breakthrough infections continue to appear, and the frequency of shingles is growing among both elderly and younger adults due to progressing lifestyle factors and immune change [5]. These biological and epidemiological complications highlight the need for mathematical models efficient of capturing long-term viral latency, nonlinear immune exchanges, and delayed reactivation procedures features that classical integer-order differential equations do not sufficiently represent.

Mathematical modeling performs as a fundamental tool for identifying the transmission dynamics and immunological processes connected with infectious diseases. Classical compartmental models traditionally use integer-order derivatives, which believe that system evolution depends solely on present states; however, many biological occurrences are inherently motivated by memory and past events. This limitation has determined the integration of fractional calculus into epidemiological modeling, as fractional operators naturally combine hereditary and temporal non locality [6]. Among the several fractional operators, the CF derivative has achieved substantial attention due to its non-singular exponential decay kernel, which describes fading memory more accurately than classical power-law kernels [7]. The CF formulation offers smoother analytical behavior, enhanced stability for numerical computation, and better applicability to real-world systems including immunity loss, viral latency, and recurrence processes [8]. In the perspective of shingles, fractional-order models specify an ideal framework for observing long-term viral dormancy, the gradual reducing of immune responses over years, and the effects of vaccination or increasing interventions. Modifying the fractional order supports researchers to explore how short and long-range memory contribute to disease transmission, recovery patterns, and the determination of infected or dormant individuals [9]. Moreover, determining the existence and uniqueness of results using fixed-point theory confirms that the fractional model performs in a mathematically sound and biologically significant manner [10]. The CF operator is predominantly suitable for computational models of complex epidemiological systems, as it enables stable numerical solutions and correctly reflects the belated physiological effects feature of herpes zoster dynamics.

In recent years, the incorporation of artificial intelligence and deep learning into fractional-order epidemiological modeling has expressively enhanced predictive accuracy and analytical depth. Fractional-order systems inherently yield nonlinear, memory-driven, and occasionally non-smooth

trajectories, formulating them well-suited for approximation through artificial neural networks (ANNs) [11]. Feedback neural networks are particularly useful for such problems because their design allows information flow from previous positions, supporting naturally with the memory properties inserted in CF fractional derivatives [12]. The Levenberg–Marquardt (LM) algorithm, widely observed as one of the most efficient training techniques for nonlinear least-squares optimization, is utilized to accelerate learning, decrease approximation error, and improve convergence stability [13]. When linked with discrete numerical iterative methods, ANNs form a hybrid analytical context in which dynamic behaviors are accurately approximated while continuing numerical consistency. This approach permits comprehensive evaluation of regression accuracy, training performance, error distribution, and predictive robustness for the fractional shingles model [14]. Moreover, ANN-assisted simulations permit detailed revelation of susceptible, vaccinated, exposed, infected, and recovered populations under special fractional orders, thereby demonstrating how memory effects influence disease burden, vaccination influence, and immunity reinforcement [15]. The interaction between fractional calculus and neural-network-based procedures represents an emerging hypothesis in mathematical epidemiology, suggesting enhanced interpret ability, greater computational accuracy, and deeper discernment into the temporal development of infectious diseases such as shingles [16].

Our work organized Figure 1, which is given.

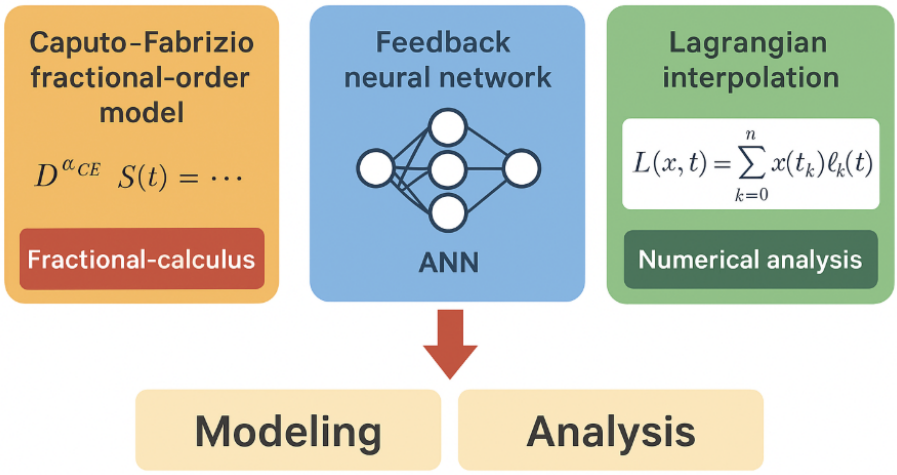

Figure 1. Organization of Caputo–Fabrizio fractional order shingles disease model.

The importance of this study:

- The study determines a unified framework that incorporates CF fractional calculus with artificial neural networking, validating how memory-driven epidemiological dynamics can be efficiently revealed through data-driven learning.
- By retaining the Levenberg–Marquardt algorithm within a feedback neural network architecture, the model attains exceptionally high accuracy and stability, showing the feasibility of ANN-based prediction for complicated viral reactivation diseases like shingles.
- The Lagrangian interpolation scheme specifies a robust numerical benchmark that confirms the neural network outputs, permitting a dual-method verification that increases the reliability of the fractional shingles model.

- The integration of vaccination fraction, natural immunity maintenance, vaccine inefficiency, advancing response, and fractional-order memory effects focuses the multi factorial mechanisms that impact shingles progression, present medically relevant insights.
- The fractional-order parameter ρ_{CF} exposes the critical role of long-term immunological memory in determining disease trajectories, presenting that fractional derivatives provide a more realistic sketch of shingles decline patterns.
- The study exhibits how ANN-driven pattern identification can enhance the interpretation of nonlinear epidemic models, requiring a foundation for future real-time checking systems and intelligent decision-support tackles in infectious disease management.
- By combining mathematical consistency with computational intelligence, the study sets a methodological precedent for operating hybrid fractional AI frames to other vaccine-preventable infections, thereby donating to a broader epidemiological modeling paradigm.

2. Preliminaries results

In this section, we give the basic views and mathematical designs from fractional calculus that form the foundation of the proposed analytical system. These definitions are crucial in relating the systems that have memory and hereditary properties, which cannot be appropriately express through integer-order operators. Consuming fractional operators, the model becomes adaptable and accurate in complicated dynamics, for more details [17–19]. The definitions described theoretical enhancements and numerical solutions in the undermentioned sections.

Definition 1. *The CF fractional operator of* $\mathbb{Y}(t)$*, let* $\mathbb{Y} \in H^1(a,b)$ *where* $b > a$ *and* $\rho \in [0,1]$ *is characterized as*

$$ {}^{CF}D_t^{\rho}\{\mathbb{Y}(t)\} = \frac{\mathbb{K}(\rho)}{1-\rho}\int_a^t \mathbb{Y}'(\theta)\exp\left[-\frac{\rho}{1-\rho}(t-\theta)\right]d\theta, \quad 0<\rho\leq 1, \tag{2.1}$$

where $\mathbb{K}(\rho)$ is a normalization function such that $\mathbb{K}(0) = \mathbb{K}(1) = 1$.

If $\mathbb{Y} \notin H^1(a,b)$, then the fractional derivative takes the following form:

$$ {}^{CF}D_t^{\rho}\{\mathbb{Y}(t)\} = \frac{\rho\mathbb{K}(\rho)}{1-\rho}\int_a^t [\mathbb{Y}(t)-\mathbb{Y}(\theta)]\exp\left[-\frac{\rho}{1-\rho}(t-\theta)\right]d\theta. \tag{2.2}$$

Remark 1. *If we define* $\sigma = \frac{1-\rho}{\rho} \in [0,\infty)$ *such that* $\rho = \frac{1}{1+\sigma} \in [0,1]$*, then Eq* (2.2) *can equivalently be rewritten as*

$$ {}^{CF}D_t^{\rho}\{\mathbb{Y}(t)\} = \frac{N(\sigma)}{\sigma}\int_a^t \mathbb{Y}'(\theta)\exp\left[-\frac{t-\theta}{\sigma}\right]d\theta, \tag{2.3}$$

where $N(0) = N(\infty) = 1$.

Definition 2. *For* $0 < \rho < 1$*, the fractional CF integral of order* ρ *for a continuous function* $\mathbb{Y}(t)$ *is defined as*

$$ {}^{CF}I_t^{\rho}\{\mathbb{Y}(t)\} = \frac{2(1-\rho)}{(2-\rho)\mathbb{K}(\rho)}\mathbb{Y}(t) + \frac{2\rho}{(2-\rho)\mathbb{K}(\rho)}\int_0^t \mathbb{Y}(q)\,dq, \quad t\geq 0,\ 0<\rho\leq 1. \tag{2.4}$$

Remark 2. *From Definitions, the following relationship holds:*

$$\frac{2(1-\rho)}{(2-\rho)\mathbb{K}(\rho)} + \frac{2\rho}{(2-\rho)\mathbb{K}(\rho)} = 1. \tag{2.5}$$

This implies that

$$\mathbb{K}(\rho) = \frac{2}{2-\rho}, \quad 0 < \rho < 1. \tag{2.6}$$

The general formulation yields a *CF derivative* of order $0 < \rho < 1$:

$${}^{CF}D_t^{\rho}\{\mathbb{Y}(t)\} = \frac{1}{1-\rho}\int_0^t \mathbb{Y}'(\theta)\exp\left[-\frac{\rho}{1\rho}(t-\theta)\right]d\theta. \tag{2.7}$$

3. Model description

The CF SVEIR model formulated above offers a mathematically enhanced representation of shingles prorogation and reactivation by inserting memory-dependent effects inherent to varicella-zoster virus biology into a fractional epidemiological structure. shingles is fundamentally distinctive from classical infectious diseases because its connective agent persists lifetime in the sensory ganglia and may reactivate years after primary infection, consequently, the CF operator, with its non-singular exponential kernel, gives a more biologically faithful mechanism for indicating this sustained immunological memory than classical integer-order models. The susceptible class $\mathcal{S}(t)$ evolves under the joint action of demographic recruitment $(1-\psi)\pi M$, exhibiting individuals entering the population without immediate immunization, and unfinished or delayed vaccination communicated through $(1-\sigma)\xi$, capturing defects in vaccine deployment or uptake. The term $(1-\zeta)\beta\mathcal{V}(t)$ explains the possibility of breakthrough infection among vaccinated individuals, allowing that shingles vaccination, while highly effective, does not deliver absolute protection against VZV reactivation. Losses from the susceptible class arise through infection pressure θ, direct vaccination ϕ_1, and natural mortality ν, presenting a comprehensive balance of biological advancement and demographic decay. The vaccinated class $\mathcal{V}(t)$ collects newly immunized creatures from demographic vaccination $\psi\pi M$, vaccination of formerly susceptible individuals $\phi_1\mathcal{S}(t)$, and external vaccination campaigns denoted by $\sigma\xi$. This class is simultaneously reduced by residual infection risk $(1-\zeta)\beta$, immunity waning portrayed by $\delta\phi_2$, and natural mortality ν. The inclusion of waning immunity is important because immune protection against VZV, even after vaccination, gradually declines with age, constructing a realistic pathway toward reactivation exposure. The visible class $\mathcal{E}(t)$ contains individuals who have confronted VZV but remain in the non-infectious incubation period; its dynamics are driven by the disclosure rate $\theta\mathcal{S}(t)$ and subsequently controlled by progression near infectiousness at rate η, balanced beside natural death ν. This compartment is vital for demonstrating the delay between primary revealing and reactivation, capturing the temporal lag in disease beginning. The infectious class $\mathcal{I}(t)$ reveals individuals experiencing active shingles episodes, getting inflow from the exposed class at rate η and outflow to the recovered class through recovery rate ι, while being concurrently subjected to demographic elimination by ν. This compartment establishes the symptomatic burden of shingles within the community and performances a central role in quantifying clinical severity, healthcare influence, and secondary transmission potential. The recovered class $\mathcal{R}(t)$ captures both

natural and vaccine-induced immunity, obtaining individuals through two distinct pathways: clinical recovery $\iota\mathcal{I}(t)$ and reinforced immunity in vaccinated individuals denoted by $\delta\phi_2\mathcal{V}(t)$.

$$\begin{aligned}
{}^{CF}D_t^{\rho}\mathcal{S}(t) &= (1-\psi)\pi M + (1-\sigma)\xi + (1-\zeta)\beta\mathcal{V}(t) - (\theta+\phi_1+\nu)\mathcal{S}(t),\\
{}^{CF}D_t^{\rho}\mathcal{V}(t) &= \psi\pi M + \sigma\xi + \phi_1\mathcal{S}(t) - ((1-\zeta)\beta + \delta\phi_2 + \nu)\mathcal{V}(t),\\
{}^{CF}D_t^{\rho}\mathcal{E}(t) &= \theta\mathcal{S}(t) - (\eta+\nu)\mathcal{E}(t),\\
{}^{CF}D_t^{\rho}\mathcal{I}(t) &= \eta\mathcal{E}(t) - (\iota+\nu)\mathcal{I}(t),\\
{}^{CF}D_t^{\rho}\mathcal{R}(t) &= \iota\mathcal{I}(t) + \delta\phi_2\mathcal{V}(t) - \nu\mathcal{R}(t).
\end{aligned} \tag{3.1}$$

Subject to the initial conditions:

$$\mathcal{S}(0) = \mathcal{S}_0, \quad \mathcal{V}(0) = \mathcal{V}_0, \quad \mathcal{E}(0) = \mathcal{E}_0, \quad \mathcal{I}(0) = \mathcal{I}_0, \quad \mathcal{R}(0) = \mathcal{R}_0. \tag{3.2}$$

Natural mortality ν eradicates individuals from this class, finalizing the demographic balance. The contact among these compartments systems a coherent system that mirrors the biological lifecycle of VZV, describing for primary infection, latency, waning immunity, aging-related repetition, and the protective effect of vaccination plans. Each parameter plays a unique mechanistic role: ψ, σ, and ϕ_1 establish the intensity and reach of immunization strategies; ϑ calculates the resilience of vaccine protection against infection; θ and β adjust exposure intensity and effect the probability of transition from susceptibility to infection; η predetermines the latency-to-reactivation process; and ι describes the clinical purpose of disease. The fractional order ρ is the most conceptually important element of the model, because it governs the degree to which historical states influence current dynamics, permitting the system to reflect the long immunological memory properties of shingles something a standard integer-order operator cannot reproduce. In practical terms, declining ρ enhances the contribution of past spotlights and immunity profiles, thus acknowledging the model to simulate realistic delays, age-related susceptibility patterns, and decline phenomena. The CF operator confirms that this memory effect is mathematically smooth and free from singular kernels, manufacture the system suitable for both analytical and numerical examinations. Collectively, the model determines a refined mathematical platform capable of estimating the long-term performance of shingles within vaccinated and un vaccinated populations, evaluating the sustainability of vaccination policies, predicting the conditions under which shingles frequency may rise due to waning immunity, and identifying critical thresholds for involvement. Through its integration of fractional dynamics, the model goes beyond conventional epidemic constructions by capturing the essential chronicity of VZV, thus present an effective tool for guiding preventive approaches and understanding the disheveled roles of immunity, vaccination, and demographic progress in shaping shingles epidemiology.

4. Existence results

In this section, we establish the existence and uniqueness for the model 3.1. To get this, we utilize a fixed-point approach, which provides a demanding framework for analyzing the construction of the model's operators. By operating the procedure of fractional integral operators as given in the foundational work [20–22], we redevelop model 3.1 in an equivalent integral form. This formulation

permits us to systematically confirm the conditions under which a unique solution exists, guaranteeing the model's mathematical consistency and offering a basis for further stability and dynamical analysis.

$$\begin{aligned}
\mathcal{S}(t) - \mathcal{S}(0) &= {}_0^{CF}I_t^{\rho}\Big\{(1-\psi)\pi M + (1-\sigma)\xi + (1-\zeta)\beta\,\mathcal{V}(t) - (\theta + \phi_1 + \nu)\,\mathcal{S}(t)\Big\},\\
\mathcal{V}(t) - \mathcal{V}(0) &= {}_0^{CF}I_t^{\rho}\Big\{\psi\pi M + \sigma\xi + \phi_1\,\mathcal{S}(t) - ((1-\zeta)\beta + \delta\phi_2 + \nu)\,\mathcal{V}(t)\Big\},\\
\mathcal{E}(t) - \mathcal{E}(0) &= {}_0^{CF}I_t^{\rho}\Big\{\theta\,\mathcal{S}(t) - (\eta + \nu)\,\mathcal{E}(t)\Big\},\\
\mathcal{I}(t) - \mathcal{I}(0) &= {}_0^{CF}I_t^{\rho}\Big\{\eta\,\mathcal{E}(t) - (\iota + \nu)\,\mathcal{I}(t)\Big\},\\
\mathcal{R}(t) - \mathcal{R}(0) &= {}_0^{CF}I_t^{\rho}\Big\{\iota\,\mathcal{I}(t) + \delta\phi_2\,\mathcal{V}(t) - \nu\,\mathcal{R}(t)\Big\}.
\end{aligned} \tag{4.1}$$

Utilizing the integration definitions, we get the below:

$$\begin{aligned}
\mathcal{S}(t) - \mathcal{S}(0) &= \frac{2(1-\rho)}{\mathbb{K}(\rho)(2-\rho)}\Big\{(1-\psi)\pi M + (1-\sigma)\xi + (1-\zeta)\beta\,\mathcal{V}(t) - (\theta + \phi_1 + \nu)\,\mathcal{S}(t)\Big\}\\
&\quad + \frac{2\rho}{\mathbb{K}(\rho)(2-\rho)}\int_0^t \Big\{(1-\psi)\pi M + (1-\sigma)\xi + (1-\zeta)\beta\,\mathcal{V}(q) - (\theta + \phi_1 + \nu)\,\mathcal{S}(q)\Big\}dq,\\
\mathcal{V}(t) - \mathcal{V}(0) &= \frac{2(1-\rho)}{\mathbb{K}(\rho)(2-\rho)}\Big\{\psi\pi M + \sigma\xi + \phi_1\,\mathcal{S}(t) - ((1-\zeta)\beta + \delta\phi_2 + \nu)\,\mathcal{V}(t)\Big\}\\
&\quad + \frac{2\rho}{\mathbb{K}(\rho)(2-\rho)}\int_0^t \Big\{\psi\pi M + \sigma\xi + \phi_1\,\mathcal{S}(q) - ((1-\zeta)\beta + \delta\phi_2 + \nu)\,\mathcal{V}(q)\Big\}dq,\\
\mathcal{E}(t) - \mathcal{E}(0) &= \frac{2(1-\rho)}{\mathbb{K}(\rho)(2-\rho)}\Big\{\theta\,\mathcal{S}(t) - (\eta + \nu)\,\mathcal{E}(t)\Big\} + \frac{2\rho}{\mathbb{K}(\rho)(2-\rho)}\int_0^t \Big\{\theta\,\mathcal{S}(q) - (\eta + \nu)\,\mathcal{E}(q)\Big\}dq,\\
\mathcal{I}(t) - \mathcal{I}(0) &= \frac{2(1-\rho)}{\mathbb{K}(\rho)(2-\rho)}\Big\{\eta\,\mathcal{E}(t) - (\iota + \nu)\,\mathcal{I}(t)\Big\} + \frac{2\rho}{\mathbb{K}(\rho)(2-\rho)}\int_0^t \Big\{\eta\,\mathcal{E}(q) - (\iota + \nu)\,\mathcal{I}(q)\Big\}dq,\\
\mathcal{R}(t) - \mathcal{R}(0) &= \frac{2(1-\rho)}{\mathbb{K}(\rho)(2-\rho)}\Big\{\iota\,\mathcal{I}(t) + \delta\phi_2\,\mathcal{V}(t) - \nu\,\mathcal{R}(t)\Big\}\\
&\quad + \frac{2\rho}{\mathbb{K}(\rho)(2-\rho)}\int_0^t \Big\{\iota\,\mathcal{I}(q) + \delta\phi_2\,\mathcal{V}(q) - \nu\,\mathcal{R}(q)\Big\}dq.
\end{aligned} \tag{4.2}$$

For the simplicity of equations, we replace as follows:

$$\begin{cases}
\Pi 1(t,\mathcal{S}) = (1-\psi)\pi M + (1-\sigma)\xi + (1-\zeta)\beta\,\mathcal{V}(t) - (\theta + \phi_1 + \nu)\,\mathcal{S}(t),\\
\Pi 2(t,\mathcal{V}) = \psi\pi M + \sigma\xi + \phi_1\,\mathcal{S}(t) - ((1-\zeta)\beta + \delta\phi_2 + \nu)\,\mathcal{V}(t),\\
\Pi 3(t,\mathcal{E}) = \theta\,\mathcal{S}(t) - (\eta + \nu)\,\mathcal{E}(t),\\
\Pi 4(t,\mathcal{I}) = \eta\,\mathcal{E}(t) - (\iota + \nu)\,\mathcal{I}(t),\\
\Pi 5(t,\mathcal{R}) = \iota\,\mathcal{I}(t) + \delta\phi_2\,\mathcal{V}(t) - \nu\,\mathcal{R}(t).
\end{cases} \tag{4.3}$$

By recognized Eq (4.3), the next step is to initiate the necessary theorem that reinforces its subsequent analytical improvement.

Theorem 1. *Let the kernels* $\Pi1, \Pi2, \Pi3, \Pi4,$ *and* $\Pi5$ *of the model 3.1, and the system* (4.3) *satisfy the Lipschitz condition given below:*

$$\|\mathcal{S}\| \leq \mathcal{S}_e, \quad \|\mathcal{V}\| \leq \mathcal{V}_e, \quad \|\mathcal{E}\| \leq \mathcal{E}_e, \quad \|\mathcal{I}\| \leq \mathcal{I}_e, \quad \|\mathcal{R}\| \leq \mathcal{R}_e.$$

Proof. To prove Lipschitz condition for each kernel.

For $\Pi1$: Let $\mathcal{S}$ and $\mathcal{S}_1$ be two functions considered. Then, we have,

$$\begin{aligned}\|\Pi1(t,\mathcal{S}) - \Pi1(t,\mathcal{S}_1)\| &= \|(1-\psi)\pi M + (1-\sigma)\xi + (1-\zeta)\beta\mathcal{V} - (\theta+\phi_1+\nu)\mathcal{S} \\ &\quad - ((1-\psi)\pi M + (1-\sigma)\xi + (1-\zeta)\beta\mathcal{V} - (\theta+\phi_1+\nu)\mathcal{S}_1)\| \\ &= (\theta+\phi_1+\nu)\,\|\mathcal{S}-\mathcal{S}_1\|.\end{aligned}$$

For $\Pi2$: Similarly, for $\mathcal{V}$ and $\mathcal{V}_1$,

$$\begin{aligned}\|\Pi2(t,\mathcal{V}) - \Pi2(t,\mathcal{V}_1)\| &= \|\phi_1(\mathcal{S}-\mathcal{S}_1) - ((1-\zeta)\beta + \delta\phi_2 + \nu)(\mathcal{V}-\mathcal{V}_1)\| \\ &\leq \phi_1\,\|\mathcal{S}-\mathcal{S}_1\| + ((1-\zeta)\beta + \delta\phi_2 + \nu)\,\|\mathcal{V}-\mathcal{V}_1\|.\end{aligned}$$

For $\Pi3$: For $\mathcal{E}$ and $\mathcal{E}_1$,

$$\|\Pi3(t,\mathcal{E}) - \Pi3(t,\mathcal{E}_1)\| = (\eta+\nu)\,\|\mathcal{E}-\mathcal{E}_1\|.$$

For $\Pi4$: For $\mathcal{I}$ and $\mathcal{I}_1$,

$$\|\Pi4(t,\mathcal{I}) - \Pi4(t,\mathcal{I}_1)\| = (\iota+\nu)\,\|\mathcal{I}-\mathcal{I}_1\|.$$

For $\Pi5$: For $\mathcal{R}$ and $\mathcal{R}_1$,

$$\|\Pi5(t,\mathcal{R}) - \Pi5(t,\mathcal{R}_1)\| \leq \iota\,\|\mathcal{I}-\mathcal{I}_1\| + \delta\phi_2\,\|\mathcal{V}-\mathcal{V}_1\| + \nu\,\|\mathcal{R}-\mathcal{R}_1\|.$$

Therefore, by defining suitable constants $\Omega_1, \Omega_2, \Omega_3, \Omega_4,$ and Ω_5 for each kernel, we have

$$\begin{aligned}\|\Pi1(t,\mathcal{S}) - \Pi1(t,\mathcal{S}_1)\| &\leq \Omega_1\,\|\mathcal{S}-\mathcal{S}_1\|, \\ \|\Pi2(t,\mathcal{V}) - \Pi2(t,\mathcal{V}_1)\| &\leq \Omega_2\,\|\mathcal{V}-\mathcal{V}_1\|, \\ \|\Pi3(t,\mathcal{E}) - \Pi3(t,\mathcal{E}_1)\| &\leq \Omega_3\,\|\mathcal{E}-\mathcal{E}_1\|, \\ \|\Pi4(t,\mathcal{I}) - \Pi4(t,\mathcal{I}_1)\| &\leq \Omega_4\,\|\mathcal{I}-\mathcal{I}_1\|, \\ \|\Pi5(t,\mathcal{R}) - \Pi5(t,\mathcal{R}_1)\| &\leq \Omega_5\,\|\mathcal{R}-\mathcal{R}_1\|.\end{aligned} \tag{4.4}$$

Hence, all kernels $\Pi1, \Pi2, \Pi3, \Pi4,$ and $\Pi5$ satisfy the Lipschitz condition. □

Using the kernels, Eq (4.2) becomes:

$$\begin{cases}\mathcal{S}(t) = \mathcal{S}(0) + \dfrac{2(1-\rho)}{\mathbb{K}(\rho)(2-\rho)}\,\Pi1(t,\mathcal{S}) + \dfrac{2\rho}{\mathbb{K}(\rho)(2-\rho)}\displaystyle\int_0^t \Pi1(q,\mathcal{S})\,dq, \\ \mathcal{V}(t) = \mathcal{V}(0) + \dfrac{2(1-\rho)}{\mathbb{K}(\rho)(2-\rho)}\,\Pi2(t,\mathcal{V}) + \dfrac{2\rho}{\mathbb{K}(\rho)(2-\rho)}\displaystyle\int_0^t \Pi2(q,\mathcal{V})\,dq, \\ \mathcal{E}(t) = \mathcal{E}(0) + \dfrac{2(1-\rho)}{\mathbb{K}(\rho)(2-\rho)}\,\Pi3(t,\mathcal{E}) + \dfrac{2\rho}{\mathbb{K}(\rho)(2-\rho)}\displaystyle\int_0^t \Pi3(q,\mathcal{E})\,dq, \\ \mathcal{I}(t) = \mathcal{I}(0) + \dfrac{2(1-\rho)}{\mathbb{K}(\rho)(2-\rho)}\,\Pi4(t,\mathcal{I}) + \dfrac{2\rho}{\mathbb{K}(\rho)(2-\rho)}\displaystyle\int_0^t \Pi4(q,\mathcal{I})\,dq, \\ \mathcal{R}(t) = \mathcal{R}(0) + \dfrac{2(1-\rho)}{\mathbb{K}(\rho)(2-\rho)}\,\Pi5(t,\mathcal{R}) + \dfrac{2\rho}{\mathbb{K}(\rho)(2-\rho)}\displaystyle\int_0^t \Pi5(q,\mathcal{R})\,dq.\end{cases} \tag{4.5}$$

Then, we introduce the recursive recipe that goes with it in the form:

$$\begin{cases} \mathcal{S}_r(t) = \dfrac{2(1-\rho)}{\mathbb{K}(\rho)(2-\rho)}\,\Pi 1(t,\mathcal{S}_{(r-1)}) + \dfrac{2\rho}{\mathbb{K}(\rho)(2-\rho)}\displaystyle\int_0^t \Pi 1(q,\mathcal{S}_{(r-1)})\,dq, \\ \mathcal{V}_r(t) = \dfrac{2(1-\rho)}{\mathbb{K}(\rho)(2-\rho)}\,\Pi 2(t,\mathcal{V}_{(r-1)}) + \dfrac{2\rho}{\mathbb{K}(\rho)(2-\rho)}\displaystyle\int_0^t \Pi 2(q,\mathcal{V}_{(r-1)})\,dq, \\ \mathcal{E}_r(t) = \dfrac{2(1-\rho)}{\mathbb{K}(\rho)(2-\rho)}\,\Pi 3(t,\mathcal{E}_{(r-1)}) + \dfrac{2\rho}{\mathbb{K}(\rho)(2-\rho)}\displaystyle\int_0^t \Pi 3(q,\mathcal{E}_{(r-1)})\,dq, \\ \mathcal{I}_r(t) = \dfrac{2(1-\rho)}{\mathbb{K}(\rho)(2-\rho)}\,\Pi 4(t,\mathcal{I}_{(r-1)}) + \dfrac{2\rho}{\mathbb{K}(\rho)(2-\rho)}\displaystyle\int_0^t \Pi 4(q,\mathcal{I}_{(r-1)})\,dq, \\ \mathcal{R}_r(t) = \dfrac{2(1-\rho)}{\mathbb{K}(\rho)(2-\rho)}\,\Pi 5(t,\mathcal{R}_{(r-1)}) + \dfrac{2\rho}{\mathbb{K}(\rho)(2-\rho)}\displaystyle\int_0^t \Pi 5(q,\mathcal{R}_{(r-1)})\,dq. \end{cases} \tag{4.6}$$

with the initial conditions:

$$\mathcal{S}(0) = \mathcal{S}_0, \quad \mathcal{V}(0) = \mathcal{V}_0, \quad \mathcal{E}(0) = \mathcal{E}_0, \quad \mathcal{I}(0) = \mathcal{I}_0, \quad \mathcal{R}(0) = \mathcal{R}_0. \tag{4.7}$$

The following equation determines how the progressive terms differ from one another which takes the form

$$\begin{aligned} \omega_{1r}(t) &= \mathcal{S}_r(t) - \mathcal{S}_{(r-1)}(t) = \frac{2(1-\rho)}{\mathbb{K}(\rho)(2-\rho)}\Big[\Pi 1(t,\mathcal{S}_{(r-1)}) - \Pi 1(t,\mathcal{S}_{(r-2)})\Big] \\ &\quad + \frac{2\rho}{\mathbb{K}(\rho)(2-\rho)}\int_0^t \Big[\Pi 1(q,\mathcal{S}_{(r-1)}) - \Pi 1(q,\mathcal{S}_{(r-2)})\Big]dq, \\ \omega_{2r}(t) &= \mathcal{V}_r(t) - \mathcal{V}_{(r-1)}(t) = \frac{2(1-\rho)}{\mathbb{K}(\rho)(2-\rho)}\Big[\Pi 2(t,\mathcal{V}_{(r-1)}) - \Pi 2(t,\mathcal{V}_{(r-2)})\Big] \\ &\quad + \frac{2\rho}{\mathbb{K}(\rho)(2-\rho)}\int_0^t \Big[\Pi 2(q,\mathcal{V}_{(r-1)}) - \Pi 2(q,\mathcal{V}_{(r-2)})\Big]dq, \\ \omega_{3r}(t) &= \mathcal{E}_r(t) - \mathcal{E}_{(r-1)}(t) = \frac{2(1-\rho)}{\mathbb{K}(\rho)(2-\rho)}\Big[\Pi 3(t,\mathcal{E}_{(r-1)}) - \Pi 3(t,\mathcal{E}_{(r-2)})\Big] \\ &\quad + \frac{2\rho}{\mathbb{K}(\rho)(2-\rho)}\int_0^t \Big[\Pi 3(q,\mathcal{E}_{(r-1)}) - \Pi 3(q,\mathcal{E}_{(r-2)})\Big]dq, \\ \omega_{4r}(t) &= \mathcal{I}_r(t) - \mathcal{I}_{(r-1)}(t) = \frac{2(1-\rho)}{\mathbb{K}(\rho)(2-\rho)}\Big[\Pi 4(t,\mathcal{I}_{(r-1)}) - \Pi 4(t,\mathcal{I}_{(r-2)})\Big] \\ &\quad + \frac{2\rho}{\mathbb{K}(\rho)(2-\rho)}\int_0^t \Big[\Pi 4(q,\mathcal{I}_{(r-1)}) - \Pi 4(q,\mathcal{I}_{(r-2)})\Big]dq, \\ \omega_{5r}(t) &= \mathcal{R}_r(t) - \mathcal{R}_{(r-1)}(t) = \frac{2(1-\rho)}{\mathbb{K}(\rho)(2-\rho)}\Big[\Pi 5(t,\mathcal{R}_{(r-1)}) - \Pi 5(t,\mathcal{R}_{(r-2)})\Big] \\ &\quad + \frac{2\rho}{\mathbb{K}(\rho)(2-\rho)}\int_0^t \Big[\Pi 5(q,\mathcal{R}_{(r-1)}) - \Pi 5(q,\mathcal{R}_{(r-2)})\Big]dq. \end{aligned} \tag{4.8}$$

Further, notice that

$$\begin{aligned}\mathcal{S}_r(t) &= \sum_{i=1}^{n} \omega_{1i}(t), \quad \mathcal{V}_r(t) = \sum_{i=1}^{n} \omega_{2i}(t), \quad \mathcal{E}_r(t) = \sum_{i=1}^{n} \omega_{3i}(t),\\ \mathcal{I}_r(t) &= \sum_{i=1}^{n} \omega_{4i}(t), \mathcal{R}_r(t) = \sum_{i=1}^{n} \omega_{5i}(t).\end{aligned} \tag{4.9}$$

Where

$$\begin{aligned}\|\omega_{1r}(t)\| = \|\mathcal{S}_r(t) - \mathcal{S}_{r-1}(t)\| = \Bigg\| &\frac{2(1-\rho)}{\mathbb{K}(\rho)(2-\rho)}\Big[\Pi 1(t, \mathcal{S}_{r-1}) - \Pi 1(t, \mathcal{S}_{r-2})\Big]\\ &+ \frac{2\rho}{\mathbb{K}(\rho)(2-\rho)} \int_0^t \Big[\Pi 1(q, \mathcal{S}_{r-1}) - \Pi 1(q, \mathcal{S}_{r-2})\Big] dq\Bigg\|.\end{aligned} \tag{4.10}$$

Employing triangular inequality, Eq (4.10) deduce to

$$\begin{aligned}\|\mathcal{S}_r(t) - \mathcal{S}_{r-1}(t)\| \leq &\frac{2(1-\rho)}{\mathbb{K}(\rho)(2-\rho)} \Big\|\Pi 1(t, \mathcal{S}_{r-1}) - \Pi 1(t, \mathcal{S}_{r-2})\Big\|\\ &+ \frac{2\rho}{\mathbb{K}(\rho)(2-\rho)} \Bigg\| \int_0^t \Big[\Pi 1(q, \mathcal{S}_{r-1}) - \Pi 1(q, \mathcal{S}_{r-2})\Big] dq\Bigg\|.\end{aligned} \tag{4.11}$$

As the kernel fulfill Lipschitz condition, we reach to

$$\begin{aligned}\|\mathcal{S}_r(t) - \mathcal{S}_{r-1}(t)\| \leq &\frac{2(1-\rho)}{\mathbb{K}(\rho)(2-\rho)} \Omega_1 \|\mathcal{S}_{r-1} - \mathcal{S}_{r-2}\|\\ &+ \frac{2\rho}{\mathbb{K}(\rho)(2-\rho)} \Omega_1 \int_0^t \|\mathcal{S}_{r-1} - \mathcal{S}_{r-2}\| dq.\end{aligned} \tag{4.12}$$

We get the following inequality

$$\|\omega_{1r}(t)\| \leq \frac{2(1-\rho)}{\mathbb{K}(\rho)(2-\rho)} \Omega_1 \|\omega_{1(r-1)}(t)\| + \frac{2\rho}{\mathbb{K}(\rho)(2-\rho)} \Omega_1 \int_0^t \|\omega_{1(r-1)}(q)\| dq. \tag{4.13}$$

For other kernal proceeding with the same:

$$\begin{aligned}\|\omega_{1r}(t)\| &\leq \frac{2(1-\rho)}{\mathbb{K}(\rho)(2-\rho)} \Omega_1 \|\omega_{1(r-1)}(t)\| + \frac{2\rho}{\mathbb{K}(\rho)(2-\rho)} \Omega_1 \int_0^t \|\omega_{1(r-1)}(q)\| dq,\\ \|\omega_{2r}(t)\| &\leq \frac{2(1-\rho)}{\mathbb{K}(\rho)(2-\rho)} \Omega_2 \|\omega_{2(r-1)}(t)\| + \frac{2\rho}{\mathbb{K}(\rho)(2-\rho)} \Omega_2 \int_0^t \|\omega_{2(r-1)}(q)\| dq,\\ \|\omega_{3r}(t)\| &\leq \frac{2(1-\rho)}{\mathbb{K}(\rho)(2-\rho)} \Omega_3 \|\omega_{3(r-1)}(t)\| + \frac{2\rho}{\mathbb{K}(\rho)(2-\rho)} \Omega_3 \int_0^t \|\omega_{3(r-1)}(q)\| dq,\\ \|\omega_{4r}(t)\| &\leq \frac{2(1-\rho)}{\mathbb{K}(\rho)(2-\rho)} \Omega_4 \|\omega_{4(r-1)}(t)\| + \frac{2\rho}{\mathbb{K}(\rho)(2-\rho)} \Omega_4 \int_0^t \|\omega_{4(r-1)}(q)\| dq,\\ \|\omega_{5r}(t)\| &\leq \frac{2(1-\rho)}{\mathbb{K}(\rho)(2-\rho)} \Omega_5 \|\omega_{5(r-1)}(t)\| + \frac{2\rho}{\mathbb{K}(\rho)(2-\rho)} \Omega_5 \int_0^t \|\omega_{5(r-1)}(q)\| dq.\end{aligned} \tag{4.14}$$

Therefore, we checked that all the kernels $\Pi 1, \Pi 2, \Pi 3, \Pi 4$, and $\Pi 5$ of the model 3.1 satisfies the Lipschitz Condition.

Theorem 2. *Assuming the conditions given below are satisfied, the fractional shingles model* (3.1)*, there exists a time* $t_0 > 0$ *such that it satisfies the below condition:*

$$\frac{2(1-\rho)}{\mathbb{K}(\rho)(2-\rho)}\,\Omega_1 + \frac{2\rho}{\mathbb{K}(\rho)(2-\rho)}\,\Omega_1\, t_0 < 1. \tag{4.15}$$

Proof. The components satisfying the Lipschitz condition are bounded for all functions $\mathcal{S}(t), \mathcal{V}(t), \mathcal{E}(t), \mathcal{I}(t), \mathcal{R}(t))$. Using the recursive technique, we get the below estimates:

$$\begin{aligned}
\|\omega_{1r}(t)\| &\le \|\mathcal{S}_0\|\left[\frac{2(1-\rho)}{\mathbb{K}(\rho)(2-\rho)}\Omega_1 + \frac{2\rho}{\mathbb{K}(\rho)(2-\rho)}\Omega_1 t\right]^r,\\
\|\omega_{2r}(t)\| &\le \|\mathcal{V}_0\|\left[\frac{2(1-\rho)}{\mathbb{K}(\rho)(2-\rho)}\Omega_2 + \frac{2\rho}{\mathbb{K}(\rho)(2-\rho)}\Omega_2 t\right]^r,\\
\|\omega_{3r}(t)\| &\le \|\mathcal{E}_0\|\left[\frac{2(1-\rho)}{\mathbb{K}(\rho)(2-\rho)}\Omega_3 + \frac{2\rho}{\mathbb{K}(\rho)(2-\rho)}\Omega_3 t\right]^r,\\
\|\omega_{4r}(t)\| &\le \|\mathcal{I}_0\|\left[\frac{2(1-\rho)}{\mathbb{K}(\rho)(2-\rho)}\Omega_4 + \frac{2\rho}{\mathbb{K}(\rho)(2-\rho)}\Omega_4 t\right]^r,\\
\|\omega_{5r}(t)\| &\le \|\mathcal{R}_0\|\left[\frac{2(1-\rho)}{\mathbb{K}(\rho)(2-\rho)}\Omega_5 + \frac{2\rho}{\mathbb{K}(\rho)(2-\rho)}\Omega_5 t\right]^r.
\end{aligned}$$

Existence of the given solutions is illustrated. Further, we proceed to grantee that the given functions are indeed results of Eq (3.1) given as:

$$\begin{aligned}
\mathcal{S}(t) - \mathcal{S}(0) &= \mathcal{S}_r(t) - A_r(t),\\
\mathcal{V}(t) - \mathcal{V}(0) &= \mathcal{V}_r(t) - B_r(t),\\
\mathcal{E}(t) - \mathcal{E}(0) &= \mathcal{E}_r(t) - C_r(t),\\
\mathcal{I}(t) - \mathcal{I}(0) &= \mathcal{I}_r(t) - D_r(t),\\
\mathcal{R}(t) - \mathcal{R}(0) &= \mathcal{R}_r(t) - E_r(t).
\end{aligned}$$

Deduce to

$$\begin{aligned}
A_r(t) &= \frac{2(1-\rho)}{\mathbb{K}(\rho)(2-\rho)}\Big[\Pi 1(q,\mathcal{S}_r) - \Pi 1(q,\mathcal{S}_{(r-1)})\Big] + \frac{2\rho}{\mathbb{K}(\rho)(2-\rho)}\int_0^t \Big[\Pi 1(q,\mathcal{S}_r) - \Pi 1(q,\mathcal{S}_{(r-1)})\Big]dq,\\
A_r(t) &\le \frac{2(1-\rho)}{\mathbb{K}(\rho)(2-\rho)}\Big|\Pi 1(t,\mathcal{S}_r) - \Pi 1(t,\mathcal{S}_{(r-1)})\Big| + \frac{2\rho}{\mathbb{K}(\rho)(2-\rho)}\int_0^t \Big|\Pi 1(q,\mathcal{S}_r) - \Pi 1(q,\mathcal{S}_{(r-1)})\Big|dq, \quad (4.16)\\
A_r(t) &\le \frac{2(1-\rho)}{\mathbb{K}(\rho)(2-\rho)}\Omega_1\|\mathcal{S}_r - \mathcal{S}_{(r-1)}\| + \frac{2\rho}{\mathbb{K}(\rho)(2-\rho)}\Omega_1\int_0^t \|\mathcal{S}_r - \mathcal{S}_{(r-1)}\|dq.
\end{aligned}$$

Recursively applying the same technique for all

$$\|A_r(t)\| \le \left(\frac{2(1-\rho)}{(2-\rho)\mathbb{K}(\rho)} + \frac{2\rho}{(2-\rho)\mathbb{K}(\rho)}t\right)^{n+1}\ \Omega_1^{n+1}\, a. \tag{4.17}$$

Then, for $t0$, such that

$$\|A_r(t)\| \leq \left(\frac{2(1-\rho)}{(2-\rho)\mathbb{K}(\rho)} + \frac{2\rho}{(2-\rho)\mathbb{K}(\rho)}t_0\right)^{n+1} \Omega_1^{n+1}\, a. \tag{4.18}$$

By employing the limit to Eq (4.18) as n tends to infinity, we get the below.
Since $\|A_r(t)\| \to 0$ as $n \to \infty$, with same approach we obtain

$$\|B_r(t)\| \to 0, \qquad \|C_r(t)\| \to 0, \qquad \|D_r(t)\| \to 0,$$

$$\|E_r(t)\| \to 0,$$

as $n \to \infty$.

Uniqueness of the results to system (3.1), consider that there exists distinct result represented by

$$\mathcal{S}_r(t), \quad \mathcal{V}_r(t), \quad \mathcal{E}_r(t), \quad \mathcal{I}_r(t), \quad \mathcal{R}_r(t),$$

correspondingly, for other compartments,

$$\mathcal{S}_{r1}(t), \quad \mathcal{L}_{r1}(t), \quad \mathcal{I}_{r1}(t), \quad \mathcal{R}_{r1}(t).$$

We reach to the below relations:

$$\mathcal{S}_r(t) - \mathcal{S}_{r1}(t) = \frac{2(1-\rho)}{\mathbb{K}(\rho)(2-\rho)}[\Pi 1(t,\mathcal{S}_r) - \Pi 1(t,\mathcal{S}_{r1})] + \frac{2\rho}{\mathbb{K}(\rho)(2-\rho)}\int_0^t [\Pi 1(q,\mathcal{S}_r) - \Pi 1(q,\mathcal{S}_{r1})]\, dq. \tag{4.19}$$

Applying the norm of Eq (4.19), we get the below inequality

$$\left\|\mathcal{S}_r(t) - \mathcal{S}_{r1}(t)\right\| \leq \frac{2(1-\rho)}{\mathbb{K}(\rho)(2-\rho)}\left\|\Pi 1(t,\mathcal{S}_r) - \Pi 1(t,\mathcal{S}_{r1})\right\| + \frac{2\rho}{\mathbb{K}(\rho)(2-\rho)}\left\|\int_0^t [\Pi 1(q,\mathcal{S}_r) - \Pi 1(q,\mathcal{S}_{r1})]\, dq\right\|.$$

$$\left\|\mathcal{S}_r(t) - \mathcal{S}_{r1}(t)\right\| \leq \frac{2(1-\rho)}{\mathbb{K}(\rho)(2-\rho)}\,\Omega_1\left\|\mathcal{S}_r - \mathcal{S}_{r1}\right\| + \frac{2\rho}{\mathbb{K}(\rho)(2-\rho)}\int_0^t \Omega_1\left\|\mathcal{S}_r - \mathcal{S}_{r1}\right\| dq. \tag{4.20}$$

Next, it follows that

$$\left\|\mathcal{S}_r(t) - \mathcal{S}_{r1}(t)\right\| \leq \Omega_1\left(\frac{2(1-\rho)}{\mathbb{K}(\rho)(2-\rho)} + \frac{2\rho}{\mathbb{K}(\rho)(2-\rho)}\,t\right)\left\|\mathcal{S}_r - \mathcal{S}_{r1}\right\|,$$

by using the kernel's Lipschitz condition, we obtain:

$$\left\|\mathcal{S}_r(t) - \mathcal{S}_{r1}(t)\right\|\left(1 - \frac{2(1-\rho)}{\mathbb{K}(\rho)(2-\rho)}\,\Omega_1 - \frac{2\rho}{\mathbb{K}(\rho)(2-\rho)}\,\Omega_1 t\right) \leq 0. \tag{4.21}$$

□

Theorem 3. *The results of the fractional model* (3.1) *for the compartments* $\mathcal{S}(t), \mathcal{V}(t), \mathcal{E}(t), \mathcal{I}(t), \mathcal{R}(t)$ *is unique solutions whenever the below condition is fulfilled:*

$$\left(1 - \frac{2(1-\rho)}{\mathbb{K}(\rho)(2-\rho)}\,\Omega_1 - \frac{2\rho}{\mathbb{K}(\rho)(2-\rho)}\,\Omega_1 t\right) > 0. \tag{4.22}$$

Proof. From inequality (4.21), the uniqueness of the susceptible component satisfies

$$\left\|\mathcal{S}(t) - \mathcal{S}_1(t)\right\| \left(1 - \frac{2(1-\rho)}{\mathbb{K}(\rho)(2-\rho)}\,\Omega_1 - \frac{2\rho}{\mathbb{K}(\rho)(2-\rho)}\,\Omega_1 t\right) \leq 0.$$

Thus, condition (4.22) ensures

$$\left\|\mathcal{S}(t) - \mathcal{S}_1(t)\right\| = 0.$$

This implies

$$\mathcal{S}(t) = \mathcal{S}_1(t).$$

Employing the same procedure to the system (3.1) for other components we get the following,

$$\mathcal{V}(t) = \mathcal{V}_1(t), \qquad \mathcal{E}(t) = \mathcal{E}_1(t), \qquad \mathcal{I}(t) = \mathcal{I}_1(t), \qquad \mathcal{R}(t) = \mathcal{R}_1(t).$$

Therefore, the system (3.1), is unique solution. □

5. Numerical method

Fractional derivatives with non-singular kernels, such as the CF derivative, have obtained significant attraction in modeling complex dynamical systems. To numerically approximate the CF derivative, Lagrange interpolation is commonly employed to estimate the derivative of the applied function [23–26]. The CF derivative of order $\rho \in (0, 1)$ for a function $\mathbb{Y}(t)$ is defined as

$${}^{CF}D^{\rho}\mathbb{Y}(t) = \frac{\mathbb{K}(\rho)}{1-\rho}\int_0^t \mathbb{Y}'(\tau)\exp\Big[-\frac{\rho}{1-\rho}(t-\tau)\Big]\,d\tau, \tag{5.1}$$

where $\mathbb{K}(\rho)$ is a normalization constant, usually the value is set to 1. This derivative using an exponential kernel, which differentiate it from classical Caputo derivatives and avoid singularities.

The CF derivative depends on the first derivative $\mathbb{Y}'(\tau)$ incorporating against an exponential weight, which shows recent history more than distant past. This requires a reliable approximation of $\mathbb{Y}'(\tau)$ over the interval $[0, t]$.

Consider a uniform grid of points $\{t_0, t_1, \ldots, t_r\}$ ans using with function values $\mathbb{Y}(t_0), \mathbb{Y}(t_1), \ldots, \mathbb{Y}(t_r)$. The linear Lagrange interpolation polynomial on each sub interval $[t_{k-1}, t_k]$ is

$$\mathbb{Y}(\tau) \approx \mathbb{Y}(t_{k-1})\frac{t_k - \tau}{h} + \mathbb{Y}(t_k)\frac{\tau - t_{k-1}}{h}, \quad \tau \in [t_{k-1}, t_k], \tag{5.2}$$

where $h = t_k - t_{k-1}$ is the uniform step size.

Differentiating of the polynomial leads to a constant derivative on each interval:

$$\mathbb{Y}'(\tau) \approx \frac{\mathbb{Y}(t_k) - \mathbb{Y}(t_{k-1})}{h}. \tag{5.3}$$

Now, Lagrange polynomial gives us to approximate $\mathbb{Y}(t)$ between two discrete points, and its derivative allows a simple estimate for $\mathbb{Y}'(\tau)$ needed in the CF integral. Using linear interpolation ensures simplicity and computational efficiency.

Substituting the interpolated derivative into the CF definition, the derivative at t_r can be approximated as a sum over subintervals:

$$ {}^{CF}D^{\rho}\mathbb{Y}(t_r) \approx \frac{\mathbb{K}(\rho)}{1-\rho}\sum_{k=1}^{r}\int_{t_{k-1}}^{t_k}\mathbb{Y}'(\tau)\exp\Big[-\vartheta(t_r-\tau)\Big]d\tau, \quad \vartheta=\frac{\rho}{1-\rho}. \tag{5.4} $$

Breaking the integral into sub intervals allows for piecewise approximation of $\mathbb{Y}'(\tau)$, which is essential because $\mathbb{Y}'(\tau)$ is generally unknown at intermediate points.

By replacing $\mathbb{Y}'(\tau)$ with its linear interpolate derivative, we have

$$ {}^{CF}D^{\rho}\mathbb{Y}(t_r) \approx \frac{\mathbb{K}(\rho)}{(1-\rho)h}\sum_{k=1}^{r}\big(\mathbb{Y}(t_k)-\mathbb{Y}(t_{k-1})\big)\int_{t_{k-1}}^{t_k}e^{-\vartheta(t_r-\tau)}d\tau. \tag{5.5} $$

The exponential integral over a sub interval can be computed analytically:

$$ \int_{t_{k-1}}^{t_k}e^{-\vartheta(t_r-\tau)}d\tau=\frac{1}{\vartheta}\Big(e^{-\vartheta(t_r-t_k)}-e^{-\vartheta(t_r-t_{k-1})}\Big). \tag{5.6} $$

Hence, the final numerical approximation for the CF derivative is

$$ {}^{CF}D^{\rho}\mathbb{Y}(t_r) \approx \frac{\mathbb{K}(\rho)}{(1-\rho)h\vartheta}\sum_{k=1}^{r}\big(\mathbb{Y}(t_k)-\mathbb{Y}(t_{k-1})\big)\Big(e^{-\vartheta(t_r-t_k)}-e^{-\vartheta(t_r-t_{k-1})}\Big). \tag{5.7} $$

This formula efficiently computes the CF derivative using only the discrete function values. The exponential kernel is exactly integrated over each sub interval, and the piecewise linear interpolation ensures that the derivative is well-approximated. This method is suitable for solving CF fractional differential equations in various applications such as epidemic modeling, fluid dynamics, and control systems.

To numerically solve the CF fractional SVEIR system (3.1), we employ a piecewise linear Lagrange interpolation method. Consider a uniform time grid

$$ t_r = rh, \quad r=0,1,\ldots,N, \quad h=\text{step size}. $$

For each compartment $X(t)\in\{\mathcal{S},\mathcal{V},\mathcal{E},\mathcal{I},\mathcal{R}\}$, the CF derivative is approximated using piecewise linear Lagrange interpolation:

$$ {}^{CF}D^{\rho}X(t_r) \approx \frac{\mathbb{K}(\rho)}{(1-\rho)h\vartheta}\sum_{k=1}^{r}(X_k-X_{k-1})\Big(e^{-\vartheta(t_r-t_k)}-e^{-\vartheta(t_r-t_{k-1})}\Big), \quad \vartheta=\frac{\rho}{1-\rho}. \tag{5.8} $$

The linear Lagrange polynomial approximates $X(t)$ on each subinterval, and its derivative is constant. Substituting into the CF integral and integrating analytically over each subinterval yields Eq (5.8), which preserves the memory effect of the fractional derivative.

Define the right-hand sides of the system as

$$ \begin{aligned} \Pi S(t_r) &= (1-\psi)\pi M + (1-\sigma)\xi + (1-\zeta)\beta\mathcal{V}_r - (\theta+\phi_1+\nu)\mathcal{S}_r,\\ \Pi V(t_r) &= \psi\pi M + \sigma\xi + \phi_1\mathcal{S}_r - ((1-\zeta)\beta+\delta\phi_2+\nu)\mathcal{V}_r,\\ \Pi E(t_r) &= \theta\mathcal{S}_r - (\eta+\nu)\mathcal{E}_r,\\ \Pi I(t_r) &= \eta\mathcal{E}_r - (\iota+\nu)\mathcal{I}_r,\\ \Pi R(t_r) &= \iota\mathcal{I}_r + \delta\phi_2\mathcal{V}_r - \nu\mathcal{R}_r. \end{aligned} $$

The fully discrete CF-Lagrange system is then

$$\frac{\mathbb{K}(\rho)}{(1-\rho)h\vartheta}\sum_{k=1}^{r}(\mathcal{S}_k-\mathcal{S}_{k-1})\Big(e^{-\vartheta(t_r-t_k)}-e^{-\vartheta(t_r-t_{k-1})}\Big)=(t_r),$$

$$\frac{\mathbb{K}(\rho)}{(1-\rho)h\vartheta}\sum_{k=1}^{r}(\mathcal{V}_k-\mathcal{V}_{k-1})\Big(e^{-\vartheta(t_r-t_k)}-e^{-\vartheta(t_r-t_{k-1})}\Big)=(t_r),$$

$$\frac{\mathbb{K}(\rho)}{(1-\rho)h\vartheta}\sum_{k=1}^{r}(\mathcal{E}_k-\mathcal{E}_{k-1})\Big(e^{-\vartheta(t_r-t_k)}-e^{-\vartheta(t_r-t_{k-1})}\Big)=(t_r),$$

$$\frac{\mathbb{K}(\rho)}{(1-\rho)h\vartheta}\sum_{k=1}^{r}(\mathcal{I}_k-\mathcal{I}_{k-1})\Big(e^{-\vartheta(t_r-t_k)}-e^{-\vartheta(t_r-t_{k-1})}\Big)=(t_r),$$

$$\frac{\mathbb{K}(\rho)}{(1-\rho)h\vartheta}\sum_{k=1}^{r}(\mathcal{R}_k-\mathcal{R}_{k-1})\Big(e^{-\vartheta(t_r-t_k)}-e^{-\vartheta(t_r-t_{k-1})}\Big)=(t_r).$$

For practical computation, each compartment can be updated explicitly as

$$X_r=X_0+\frac{(1-\rho)h}{\mathbb{K}(\rho)}\sum_{k=1}^{r}(t_{k-1})\Big(e^{-\vartheta(t_r-t_k)}-e^{-\vartheta(t_r-t_{k-1})}\Big),\quad X\in\{\mathcal{S},\mathcal{V},\mathcal{E},\mathcal{I},\mathcal{R}\}.$$

This forward evaluation uses the previous values of all compartments and incorporates the exponential memory kernel of the CF derivative. The piecewise linear interpolation ensures the derivative is approximated accurately on each subinterval, enabling stable and efficient numerical computation of the SEVIR system.

6. Neural networking of the model

The CF fractional-order modeling framework offers a non-singular, exponentially decaying memory kernel that is particularly suitable for representing the reactivation behavior of shingles, a disease in which the latent VZV exhibits long-term memory-driven dynamics, prompting the need for fractional calculus to capture such temporal dependence. One can see details in [27, 28].

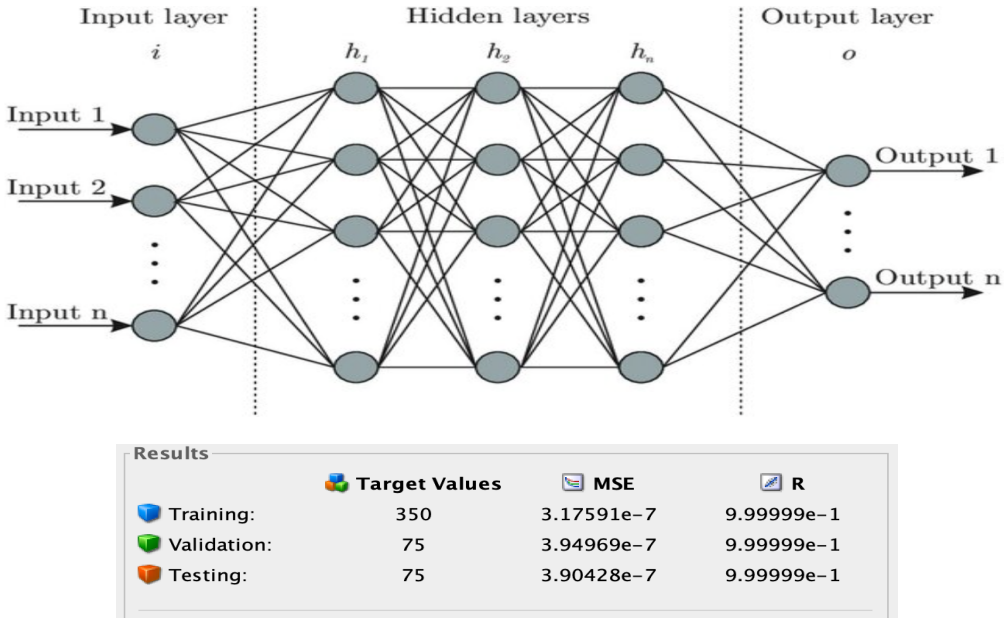

Figure 2. Feedback neural networking of system (3.1) model.

To approximate these nonlinear fractional dynamics, we employ a feedback neural network (FNN) Figure 2, capable of storing short- and long-term temporal dependencies. Let $\mathcal{Z}(t) = [\mathcal{S}(t), \mathcal{V}(t), \mathcal{E}(t), \mathcal{I}(t), \mathcal{R}(t)]^\tau$ denote the input and $\mathcal{Q}(t)$ the internal feedback state defined by

$$\mathcal{Q}(t) = \psi_1(W_h\mathcal{Z}(t) + U_h\mathcal{Q}(t-1) + b_h), \qquad \hat{\mathcal{Z}}(t) = \psi_2(W_o\mathcal{Q}(t) + b_o),$$

where $\psi_1(\cdot)$ and $\psi_2(\cdot)$ are activation functions, W_h, U_h, and W_o denote weight matrices, and b_h, b_o represent bias vectors. The training objective minimizes the mean-square error

$$E = \frac{1}{N}\sum_{k=1}^{N} \|\mathcal{Z}(t_k) - \hat{\mathcal{Z}}(t_k)\|^2.$$

Parameter updates follow the Levenberg–Marquardt (LM) rule,

$$L_{\text{new}} = L_{\text{old}} - (\phi^\top\phi + \Omega I)^{-1}\phi^\top e,$$

where ϕ is the Jacobian of residuals, e the error vector, and Ω the damping constant ensuring a smooth balance between Gauss–Newton curvature approximation and gradient-descent stability. The FNN was trained with epochs = 1000, time = 0 : 07 : 07, performance = 3.18×10^{-7}, gradient = 1.21×10^{-4}, $\Omega = 1.00\times10^{6}$, and dataset partitioning of training = 375, validation = 75, and testing = 75, confirming extremely strong convergence and negligible generalization error.

The performance curve Figure 3, demonstrates that the mean-square error falls rapidly to the order of 10^{-7}, indicating that the LM algorithm efficiently adapts the network to the memory-induced nonlinearity of the CF system. The validation and test curves run nearly parallel to the training curve, exhibiting strong generalization and absence of overfitting.

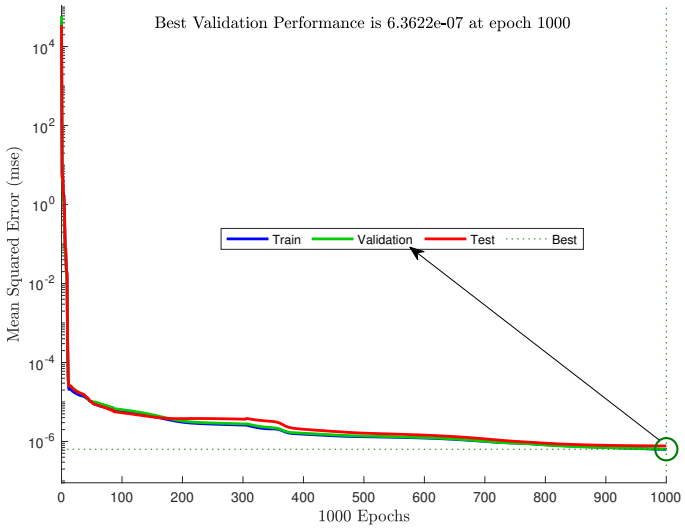

Figure 3. Best validation performance of the system (3.1) for different fractional order values.

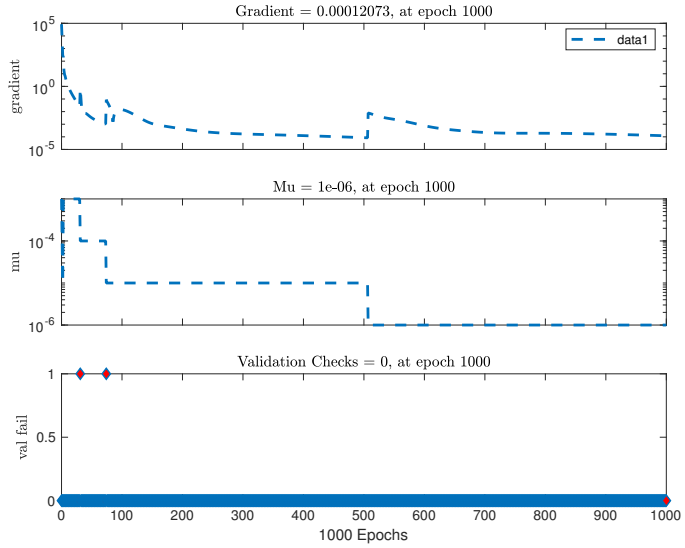

Figure 4. Training state of the system (3.1) for different fractional order values.

The training state plot Figure 4, illustrates the evolution of gradient, damping factor Ω, and validation checks; the gradient steadily decreases below 10^{-4}, confirming a stable error surface shaped by the exponentially fading CF memory kernel, while the damping parameter stabilizes near 10^{6}, indicating optimal LM convergence.

The error histogram (Figure 5 displays a narrow, symmetric distribution of residuals concentrated around zero, reflecting near-perfect reconstruction of the CF-generated trajectories; this tightly clustered profile further demonstrates the network's ability to capture the interaction between latent reactivation and infectious progression. The Regression plot Figure 6, shows correlation coefficients approaching $R \approx 1$ across training, validation, and testing, signifying an almost ideal linear relationship between predicted outputs and the true fractional-order system.

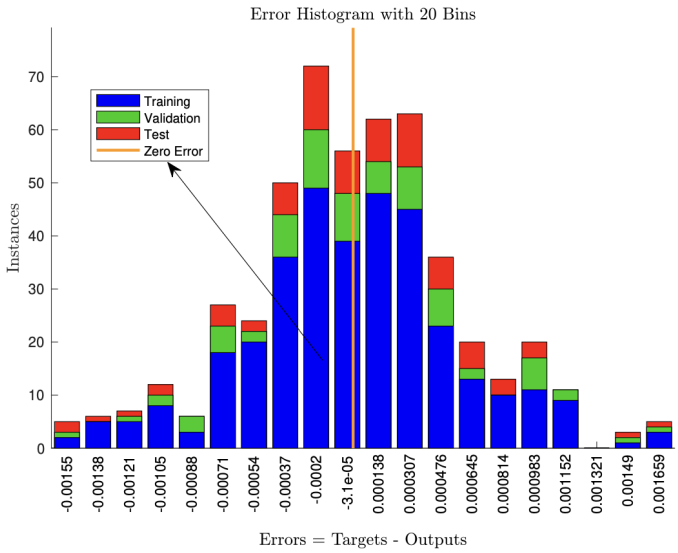

Figure 5. Training error histogram of the system (3.1) for different fractional order values.

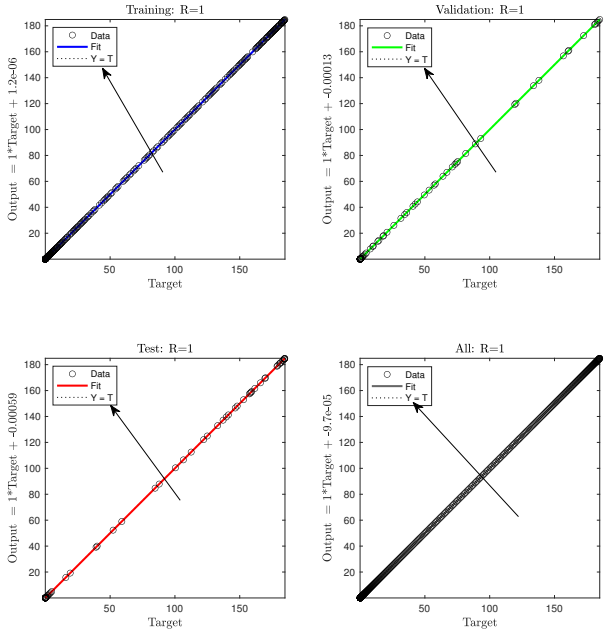

Figure 6. Training regression of the system (3.1) for different fractional order values.

Meanwhile, the time-series response Figure 7 reveals perfect overlap between predicted curves and actual CF dynamics, highlighting the network's ability to track reactivation transients and memory-driven viral behavior governed by the fractional operator. Collectively, the exceedingly small final performance value (3.18×10^{-7}), extremely low gradient (1.21×10^{-4}), and strong regression fit validate the rigorous accuracy of this hybrid CF–FNN framework. The synergy between the CF fractional structure and LM-optimized feedback neural networks provides a powerful scientific tool for predicting shingles outbreaks, analyzing latency-to-infectious transitions, and understanding the memory-driven virological processes that classical integer-order models fail to capture, establishing this methodology as a high-fidelity, computationally intelligent approach for fractional epidemiological modeling.

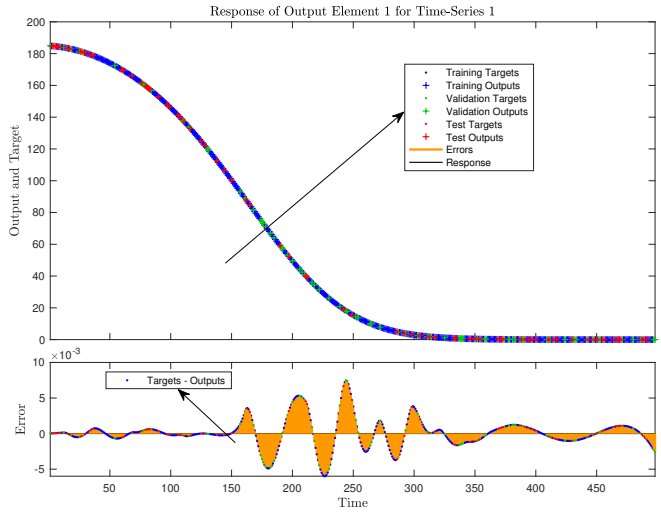

Figure 7. Time series response of the system (3.1) for different fractional order values.

7. Numerical analysis of the model

The CF fractional-order shingles disease model provides a refined mathematical structure for representing the memory-dependent reactivation dynamics of the varicella-zoster virus, and its numerical solution through the Lagrangian interpolation method enables smooth, high-accuracy approximations of the trajectories for the susceptible $\mathcal{S}(t)$, vaccinated $\mathcal{V}(t)$, exposed $\mathcal{E}(t)$, infected $\mathcal{I}(t)$, and recovered $\mathcal{R}(t)$ populations under clinically relevant parameters in Table 1. CF fractional SVEIR model, the parameter σ normalizes the balance between continued vaccine-induced immunity and the ongoing return to susceptibility. Biologically, changes in σ reflect differences in immune resilience and age-related immune weakening. Smaller values of σ reveal extended immune protection, meaning vaccinated individuals reserve effective defense for longer stages. In contrast, larger σ values communicate to faster immune decline, dependable with immunosenescence and concentrated adaptive immune effectiveness in aging populations. Since the CF operator combines a non-singular fading memory kernel, previous immune conditions continue to guidance current disease dynamics. Therefore, increasing σ develops susceptibility restoration, prolongs infection persistence, and changes the long-term qualitative performance of the system. The CF derivative of order $\rho = 0.95$ incorporates an exponentially fading memory kernel consistent with the medical understanding that immunity to

shingles weakens gradually over decades, rather than abruptly, due to immunosenescence and long-term waning of varicella immunity. The model considers vaccination, boosting, natural immunity, infection transmission, and reactivation processes governed by: vaccination fraction $\psi = 0.15$, immunity fraction $\sigma = 0.10$, vaccine inefficiency $\zeta = 0.30$, recruitment rate $\pi = 20$ with scale $M = 1$, immunity gain rate $\xi = 2$, vaccine infection transmission $\beta = 0.40$, infection force from susceptible $\theta = 0.05$, vaccination rate $\phi_1 = 0.03$, boosting rate $\phi_2 = 0.04$, progression rate $\eta = 0.12$, recovery rate $\iota = 0.20$, boosting coefficient $\delta = 0.04$, and natural mortality $\nu = 0.01$. Initial conditions are $\mathcal{S}(0) = 900$, $\mathcal{V}(0) = 50$, $\mathcal{E}(0) = 20$, $\mathcal{I}(0) = 10$, and $\mathcal{R}(0) = 5$. To approximate the CF fractional dynamics numerically, the Lagrangian polynomial $L(x,t) = \sum_{k=0}^{n} x(t_k)\ell_k(t)$, where $\ell_k(t) = \prod_{j\neq k} \frac{t-t_j}{t_k-t_j}$, is employed to generate smooth trajectories across time nodes for each state variable, enabling reconstruction of the fractional memory effects without loss of accuracy.

Table 1. Caputo–Fabrizio fractional order shingles model parameter values.

Symbol	Value	Meaning	Biological interpretation
Initial Conditions			
ρ	0.95	Fractional order	memory-driven intensity
$\mathcal{S}(0)$	900	Susceptible population	individuals at risk of shingles
$\mathcal{V}(0)$	50	Vaccinated population	immunized individuals
$\mathcal{E}(0)$	20	Exposed population	latent virus carriers
$\mathcal{I}(0)$	10	Infectious population	active shingles cases
$\mathcal{R}(0)$	5	Recovered population	naturally immune individuals
Model Parameters			
ψ	0.15	Vaccination fraction	entry into vaccinated class
σ	0.10	Immunity retention factor	controls transition strength
M	1	Normalization constant	recruitment scaling factor
ξ	2	External transition term	constant transition contribution
ζ	0.30	Vaccine protection factor	reduces effective transmission
π	20	Recruitment rate	population inflow rate
η	0.12	Progression rate	latent to infectious transition
ι	0.20	Recovery rate	infectious recovery rate
β	0.4	Transmission rate	contact infection intensity
θ	0.05	Exposure rate	susceptible to exposed rate
δ	0.04	Vaccine waning rate	loss of vaccine immunity
ν	0.01	Natural death rate	background mortality
ϕ_1	0.03	Vaccination uptake rate	movement to vaccinated class
ϕ_2	0.04	Immunity boosting rate	strengthens vaccine protection

The susceptible class Figure 8, shows an initial decline driven by vaccination flow $\phi_1\mathcal{S}$, infection pressure $\theta\mathcal{S}\mathcal{I}$, and the balance between recruitment $\pi_{\text{val}}M$ and natural mortality. In a medical context, the susceptible class is influenced strongly by recruitment and natural immunity fraction σ since shingles does not spread rapidly between individuals; rather, susceptibility is shaped by immune system weakening with age. The vaccinated class Figure 9 increases due to $\phi_1\mathcal{S}$ and boosting $\phi_2\mathcal{V}$, but vaccine inefficiency $\zeta = 0.30$ channels a fraction of vaccinated individuals toward the exposed

class. Medically, this parameter is essential because shingles vaccines significantly reduce but do not completely eliminate reactivation risk; hence, ϑ determines long-term epidemiological stability in older populations.

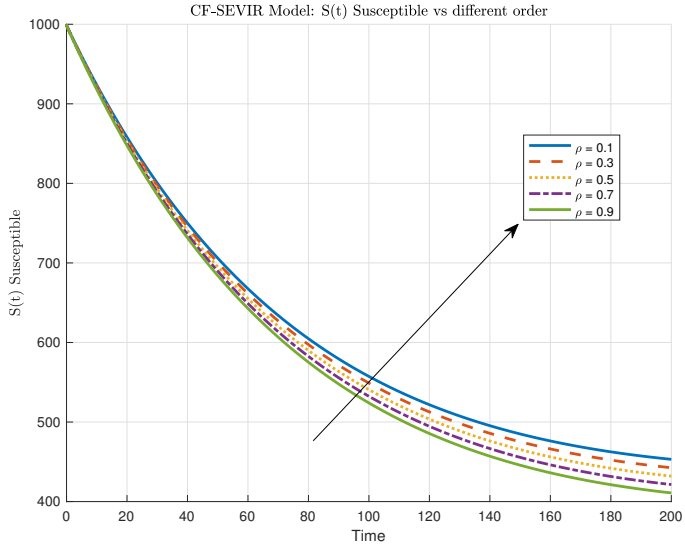

Figure 8. Susceptible class of the system (3.1) for different fractional order values.

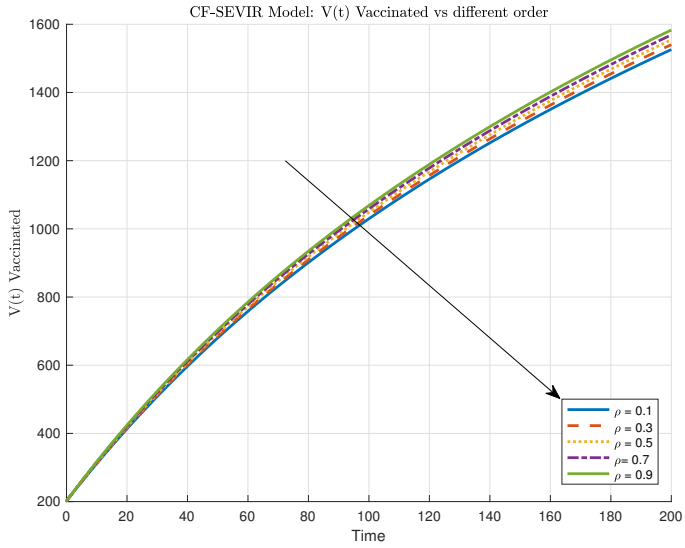

Figure 9. Vaccinated class of the system (3.1) for different fractional order values.

The exposed class Figure 10, evolves under the influence of immunity loss $\sigma\mathcal{S}$, weakening vaccine protection, and the infected-vaccinated transmission $\beta\mathcal{V}\mathcal{I}$, while the progression rate $\eta = 0.12$ directly governs how quickly latent virus reactivates to clinical shingles. From a medical viewpoint, η is among the most critical parameters because shingles arises when dormant varicella reactivates, making the exposed-to-infected transition biologically meaningful. Algorithm 1, Lagrangian interpolation

produces a smooth increase followed by stabilization, reflecting that fractional memory $\rho = 0.95$ dampens abrupt changes and models the gradual nature of shingles onset. The infected class Figure 11 represents active shingles cases and is driven by progression $\eta\mathcal{E}$, recovery $\iota\mathcal{I}$, and fractional-memory-driven dynamics.

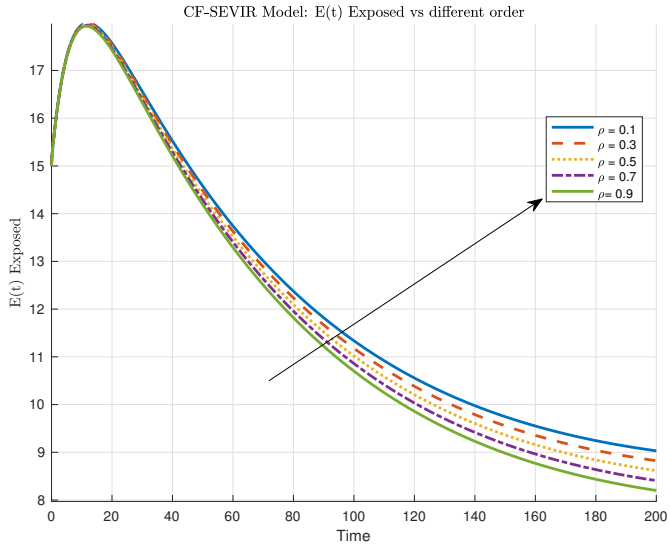

Figure 10. Exposed class of the system (3.1) for different fractional order values.

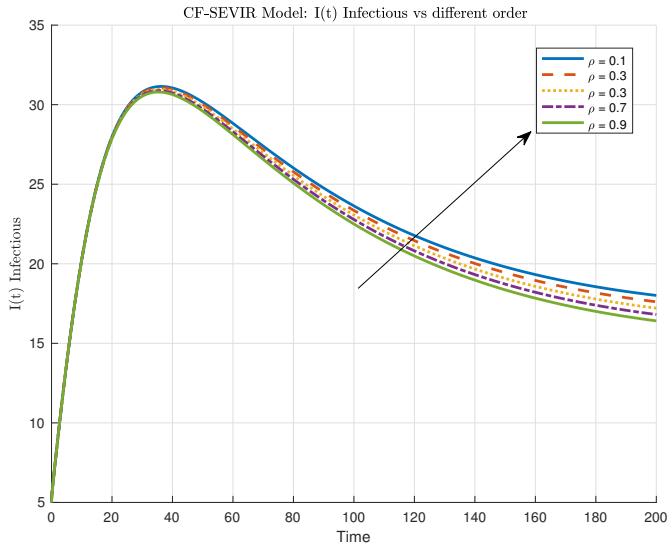

Figure 11. Infected class of the system (3.1) for different fractional order values.

Algorithm 1: Proposed algorithm

Input: X_0, Δt, T, ε

$X(0) = X_0$, $N = T/\Delta t$, $t_k = k\Delta t$

Compute a_{CF}, b_{CF}

for $k = 1 : N$

Construct $\mathcal{L}_{k-1}(t)$ from $\{X(t_j)\}_{j=0}^{k-1}$

$$\mathcal{I}_k = \int_0^{t_k} F(\mathcal{L}_{k-1}(\tau))\, d\tau$$

$X^{(0)} = X(t_{k-1})$

repeat

$X^{(m+1)} = X(0) + a_{CF}F(X^{(m)}) + b_{CF}\mathcal{I}_k$

until $\|X^{(m+1)} - X^{(m)}\|_\infty < \varepsilon$

$X(t_k) = X^{(m+1)}$

end for

Output $\{X(t_k)\}$

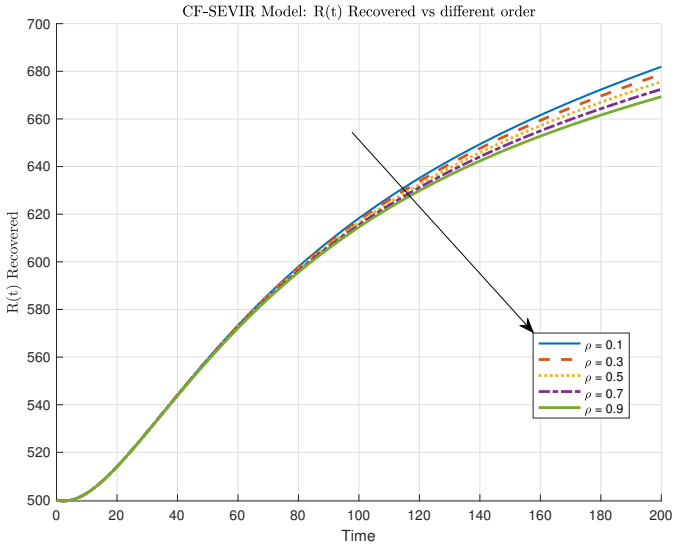

Figure 12. Recovered class of the system (3.1) for different fractional order values.

The Lagrangian approximation reveals a moderate and stable infected trajectory consistent with clinical patterns, as shingles is not a rapidly spreading epidemic but a reactivation disease found predominantly in older adults. The recovery rate $\iota = 0.20$ is medically significant because antiviral therapies can shorten the symptomatic period and reduce complications such as post-herpetic neuralgia. The recovered class Figure 12 accumulates through $\iota\mathcal{I}$ and immunity reinforcement via $\nu\mathcal{R}$, showing a gradual rise consistent with memory retention and waning governed by the CF operator. Medically important parameters in this model include the vaccination rate ϕ_1 and boosting rate ϕ_2, which influence long-term immunity levels; vaccine inefficiency ϑ, which determines breakthrough reactivation; natural immunity fraction σ, which controls susceptibility in aging populations; and progression rate η, the key determinant of clinical shingles onset. The fractional-order parameter $\rho = 0.95$ is also biologically

relevant because it reflects how historical immunity shapes present infection risk. The numerical results show that the combined CF-Lagrangian framework captures both immediate epidemiological transitions and long-memory effects, providing a realistic and medically consistent representation of shingles dynamics under vaccination and boosting strategies.

8. Conclusions

In this study, a comprehensive analytical and computational investigation of the CF fractional-order shingles transmission model was conducted by integrating two high-fidelity methodological frameworks, namely the artificial neural networking approach based on a feedback neural network trained via the Levenberg–Marquardt optimization scheme, and a precise numerical approximation constructed through the Lagrangian interpolation method, allowing for a robust cross-verification of the dynamical behavior of the epidemiological compartments. The ANN-based analysis demonstrated exceptional convergence characteristics, as reflected by the recorded performance value of 3.18×10^{-7}, a minimal gradient of 1.21×10^{-4}, and a stability-inducing damping factor $\Omega = 10^6$, achieved after 1000 epochs within a computation time of 0:07:07, while the dataset partitioning into 375 training, 75 validation, and 75 testing points further ensured predictive generalization and minimized overfitting. The performance curve, training-state evolution, error-histogram distribution, regression mapping, and time-series response collectively verified that the neural network successfully learned the intrinsic nonlinearities induced by the fractional-order operator, confirming the ability of the CF derivative to embed memory dependence and long-range correlations inherent in shingles epidemiology. Complementarily, the Lagrangian interpolation formulation, applied to the variables $\mathcal{S} = 900$, $\mathcal{V} = 50$, $\mathcal{E} = 20$, $\mathcal{I} = 10$, and $\mathcal{R} = 5$ under the parameter set $\psi = 0.15$, $\sigma = 0.10$, $\zeta = 0.30$, $\pi = 20$, $M = 1$, $\xi = 2$, $\beta = 0.4$, $\theta = 0.05$, $\phi_1 = 0.03$, $\phi_2 = 0.04$, $\eta = 0.12$, $\iota = 0.20$, $\delta = 0.04$, $\nu = 0.01$, and $\rho = 0.95$, offered an accurate reconstruction of the fractional dynamical trajectory of the susceptible, vaccinated, exposed, infected, and recovered populations, illustrating how local interpolation polynomials capture the smooth evolution of infection progression in the presence of vaccination, natural immunity, and reinfection pathways. From a medical and biological standpoint, the parameters governing vaccination fraction (ψ), natural immunity retention (σ), vaccine inefficiency (ϑ), transmission intensity under vaccination (β), and strengthening immunity through boosting (ϕ_2) were found to be crucial determinants in shaping the outbreak amplitude and persistence of shingles, while the fractional order ρ emerged as a scientifically significant quantity encapsulating the memory-driven relapse tendencies associated with varicella–zoster viral reactivation. The recovery coefficient ι and progression rate η also played decisive roles by influencing the rate at which latent infections transition toward active shingles manifestations. Collectively, the coupling of ANN-driven learning with interpolation-based numerical reconstruction provides an enriched, dual-layered perspective that enhances both predictive capacity and theoretical understanding of fractional epidemiological structures. The findings underscore the importance of fractional calculus and machine learning synergy in clinical epidemiology, demonstrating that models endowed with memory kernels and supported by data-driven training pipelines can substantially improve the interpretation, prediction, and potential control strategies for complex infections such as shingles, especially when vaccination behavior, waning immunity, and reinfection mechanisms are simultaneously present, thus establishing a rigorous scientific basis for future real-time surveillance, intervention optimization, and therapeutic

planning.

Author contributions

Aziz Khan: Writing-original draft, methodology; Aiman Mukheimer: Supervision, methodology, writing-original draft; Thabet Abdeljawad: Visualization, methodology, writing-original draft; Rajermani Thinakaran: Visualization, software, writing-original draft, writing-original draft. All authors have read and approved the final version of the manuscript for publication.

Use of Generative-AI tools declaration

The authors declare they have not used Artificial Intelligence (AI) tools in the creation of this article.

Acknowledgments

Aziz Khan, Aiman Mukheimer, and Thabet Abdeljawad would like to thank Prince Sultan University for paying the APC and for the support through TAS research lab.

Conflict of interest

There is no conflict of interest.

References

1. C. Glynn, G. Crockford, D. Gavaghan, P. Cardno, D. Price, J. Miller, Epidemiology of shingles, *J. Roy. Soc. Med.*, **83** (1990), 617–619. https://doi.org/10.1177/014107689008301007
2. N. R. Glassman, shingles, *J. Cons. Hlth. Internet*, **14** (2010), 423–433. https://doi.org/10.1080/15398285.2010.524126
3. P. Sampathkumar, L. A. Drage, D. P. Martin, Herpes zoster (shingles) and postherpetic neuralgia, *Mayo Clin. Proc.*, **84** (2009), 274–280. https://doi.org/10.4065/84.3.274
4. M. H. Motswaledi, Herpes zoster (shingles), *S. Afr. Fam. Pract.*, **60** (2018), 28–30.
5. E. Rafferty, W. McDonald, W. C. Qian, N. D. Osgood, A. Doroshenko, Evaluation of the effect of chickenpox vaccination on shingles epidemiology using agent-based modeling, *PeerJ*, **6** (2018), e5012. https://doi.org/10.7717/peerj.5012
6. B. C. Agbata, R. Dervishi, M. Gümüş, A. Smerat, G. C. E. Mbah, Analysis of fractional-order model for the transmission dynamics of malaria via Caputo–Fabrizio and Atangana–Baleanu operators, *Sci. Rep.*, **15** (2025), 36359. https://doi.org/10.1038/s41598-025-20191-7
7. I. Ahmed, A. Akgül, F. Jarad, P. Kumam, K. Nonlaopon, A Caputo–Fabrizio fractional-order cholera model and its sensitivity analysis, *Mathematical Modelling and Numerical Simulation with Applications*, **3** (2023), 170–187.

8. R. Jan, Z. Shah, N. Vrinceanu, M. H. Alshehri, N. N. A. Razak, M. Racheriu, Fractional view analysis of the dynamics of a plant disease through Caputo–Fabrizio derivative, *Fractals*, **33** (2025), 2540079. https://doi.org/10.1142/S0218348X25400791

9. I. Ahmad, R. Jan, N. N. A. Razak, A. Khan, T. Abdeljawad, Numerical investigation of the dynamical behavior of hepatitis B virus via Caputo–Fabrizio fractional derivative, *Eur. J. Pure Appl. Math.*, **18** (2025), 5509. https://doi.org/10.29020/nybg.ejpam.v18i1.5509

10. J. Z. Ndendya, J. A. Mwasunda, S. Edward, N. Shaban, A Caputo–Fabrizio fractional-order model with MCMC estimation for rabies transmission dynamics in a multi-host population, *Scientific African*, **29** (2025), e02885. https://doi.org/10.1016/j.sciaf.2025.e02885

11. H. Khan, M. Abdel-Aty, D. K. Almutairi, J. F. Gómez-Aguilar, J. Alzabut, Artificial intelligence neural networking for data clustering of carbon dioxide model, *Ain Shams Eng. J.*, **16** (2025), 103460. https://doi.org/10.1016/j.asej.2025.103460

12. H. Khan, J. Alzabut, M. Tounsi, D. K. Almutairi, AI-Based data analysis of contaminant transportation with regression of oxygen and nutrients measurement, *Fractal Fract.*, **9** (2025), 125. https://doi.org/10.3390/fractalfract9020125

13. H. Khan, W. F. Alfwzan, J. Alzabut, D. K. Almutairi, M. A. Azim, R. Thinakaran, Artificial intelligence and neural networking for an analysis of fractal-fractional Zika virus model, *Fractals*, **33** (2025), 25401437. https://doi.org/10.1142/S0218348X25401437

14. H. Khan, J. Alzabut, D. K. Almutairi, W. K. Alqurashi, The use of artificial intelligence in data analysis with error recognitions in liver transplantation in HIV-AIDS patients using modified ABC fractional order operators, *Fractal Fract.*, **9** (2024), 16. https://doi.org/10.3390/fractalfract9010016

15. H. Khan, M. Aslam, A. H. Rajpar, Y. M. Chu, S. Etemad, S. Rezapour, et al., A new fractal-fractional hybrid model for studying climate change on coastal ecosystems from the mathematical point of view, *Fractals*, **32** (2024), 2440015. https://doi.org/10.1142/S0218348X24400152

16. H. Khan, J. Alzabut, A. Shah, Z. Y. He, S. Etemad, S. Rezapour, et al., On fractal-fractional waterborne disease model: A study on theoretical and numerical aspects of solutions via simulations, *Fractals*, **31** (2023), 2340055. https://doi.org/10.1142/S0218348X23400558

17. D. Baleanu, A. Jajarmi, H. Mohammadi, S. Rezapour, A new study on the mathematical modelling of human liver with Caputo–Fabrizio fractional derivative, *Chaos Soliton. Fract.*, **134** (2020), 109705. https://doi.org/10.1016/j.chaos.2020.109705

18. M. Caputo, M. Fabrizio, A new definition of fractional derivative without singular kernel, *Progr. Fract. Differ. Appl.*, **1** (2015), 73–85.

19. S. Boulaaras, R. Jan, A. Khan, M. Ahsan, Dynamical analysis of the transmission of dengue fever via Caputo–Fabrizio fractional derivative, *Chaos Soliton. Fract.*, **8** (2022), 100072. https://doi.org/10.1016/j.csfx.2022.100072

20. H. Khan, A. Khan, T. Abdeljawad, A. Alkhazzan, Existence results in Banach space for a nonlinear impulsive system, *Adv. Differ. Equ.*, **2019** (2019), 18. https://doi.org/10.1186/s13662-019-1965-z

21. H. Khan, J. Alzabut, A. Shah, S. Etemad, S. Rezapour, C. Park, A study on the fractal-fractional tobacco smoking model, *AIMS Mathematics*, **7** (2022), 13887–13909. https://doi.org/10.3934/math.2022767

22. H. Khan, J. Alzabut, J. F. Gómez-Aguilar, P. Agarwal, Piecewise mABC fractional derivative with an application, *AIMS Mathematics*, **8** (2023), 24345–24366. https://doi.org/10.3934/math.20231241

23. Ç. Candan, An efficient filtering structure for Lagrange interpolation, *IEEE Signal Proc. Let.*, **14** (2007), 17–19. https://doi.org/10.1109/LSP.2006.881528

24. H. Ahmadi, A numerical scheme for advection dominated problems based on a Lagrange interpolation, *Groundwater for Sustainable Development*, **13** (2021), 100542. https://doi.org/10.1016/j.gsd.2020.100542

25. N. Yogeesh, S. I. Mohammad, J. Divyashree, N. Raja, A. Vasudevan, H. L. Long, Pesticide residue induced hepatotoxicity: Determination for animal studies based on fuzzy logic, *Appl. Math. Inform. Sci.*, **19** (2025), 365–378. http://doi.org/10.18576/amis/190212

26. M. Farman, A. Talib, K. S. Nisar, A. Sambas, M. Bayram, M. Hafez, Investigation of ABPV predict dynamics infection in honeybee colony production: Soft patterns multiscale modeling with fractional approach, *Ain Shams Eng. J.*, **16** (2025), 103626. https://doi.org/10.1016/j.asej.2025.103626

27. P. Giudici, A. Piergallini, M. C. Recchioni, E. Raffinetti, Explainable artificial intelligence methods for financial time series, *Physica A*, **655** (2024), 130176. https://doi.org/10.1016/j.physa.2024.130176

28. P. Giudici, V. Kolesnikov, SAFE AI metrics: An integrated approach, *Machine Learning with Applications*, **23** (2026), 100821. https://doi.org/10.1016/j.mlwa.2025.100821

AIMS Press